Macromodeling of Mutual Inductance for Displaced Coils Based on Laplace's Equation

Harry Weber, Harun Baran, Fabian Utermöhlen and Christian Schuster, *Senior Member, IEEE*

***Abstract*—Magnetic coupling is applied in a vast of different applications like sensors or medical imaging. Especially for inductive position sensors, magnetic coupling is a main aspect. Hereby, the position information is coded in the mutual inductance between a coil and a target. Consequently, the change of mutual inductance according to the relative position of coupled coils is of special interest in such applications. In this contribution, a new generalized method is presented which can be used to derive a macro model describing the mutual inductance with respect to relative position of a pair of coils. In contrast to the known procedures, the presented method can be applied for complex coil geometries since no analytic solution of the mutual inductance is necessary. For this purpose, it is utilized that the mutual inductance for a pair of coils can be treated as potential function which obeys Laplace's equation. By solving Laplace's equation, a physics-based approach for a macro model is derived which describes explicitly the behavior of the mutual inductance in dependency of the relative position of the coils. With this macro model, further analysis can be performed in circuit design or performance analysis of the sensor for example. For evaluation, the accuracy of the procedure is presented for different coil geometries which are applied in industrial and biomedical applications in order to emphasize the broad applicability of the presented method.**

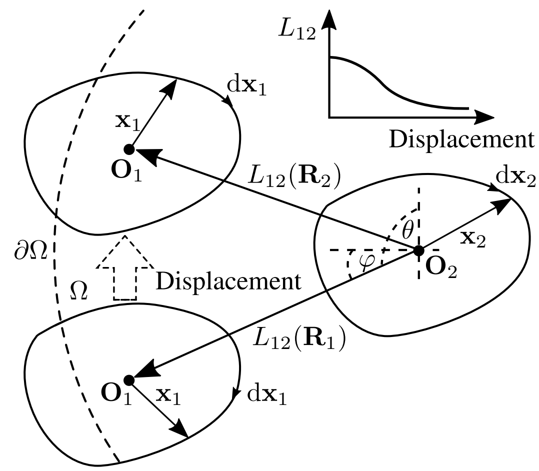

Fig. 1: Arrangement of two displaced filamentary coils with separated origins $\mathbf{O}_1$ and $\mathbf{O}_2$ for the calculation of the mutual inductance L_{12} at two different positions $\mathbf{R}_1$ and $\mathbf{R}_2$ inside a region Ω with the border $\partial\Omega$.

I. Introduction

The magnetic coupling of coils routinely plays a role in engineering applications. For example, in contactless position sensors, which are widely applied in different industrial and automotive applications, the magnetic coupling between special designed coils is used for position measuring [1]–[4]. One possible realization of such contactless position sensor is the so called Contactless Inductive Position Sensor (CIPOS®) which is applied in automotive applications. Such position sensor consists of a conductive rotor, which can be modeled as a coil, and excitation as well as receiving coils on a printed circuit board (PCB). Due to the special geometric design of the rotor and the receiving coils, the magnetic coupling between these coils changes in dependency of the relative position. A detailed description of the CIPOS® and exemplary applications can be found in [5]. For such an inductive position sensor, the behavior of the magnetic coupling mainly influences the overall performance of the sensor like accuracy or sensitivity to misalignment.

Other examples in which magnetic coupling is important can be found also in biomedical applications like magnetic resonance imaging (MRI) [6]. All these different areas of applications have in common that an appropriate model with respect to the relative position of the pair of coils is desirable. In Fig. 1, the general problem of two magnetic coupled coils is presented which are displaced to each other. The magnetic coupling of coils is described by the mutual inductance L_{12} which depends on the geometry and relative position $\mathbf{R}$ of the coils. In the case of a displacement, a change in L_{12} can be noticed as shown qualitatively in Fig. 1. In order to calculate L_{12}, usually numerical simulations or measurements are performed. However, the simulation has to be repeated for all possible relative positions of the coils. Usually, a large number of numerical simulations has to be performed. Especially, when different coil parameters are varied, this approach can be time consuming.

Alternatively, the mutual inductance can be represented by elliptic integrals using Neuman's formula which have to be solved numerically for each position [7], [8]. In dependency of the specific geometry of the coils, the numerical evaluation of these elliptic integrals can be also time consuming [9].

Another approach is to derive a so called macro model which depends only on specific parameters. In comparison to a complete model which describes the behavior in dependency of all possible parameters, like specific geometry of the coils, a macro model depends explicitly only on selected variables like the relative position of the coils. In literature, different

H. Weber, H. Baran and F. Utermöhlen are with Hella GmbH & Co. KGaA., Lippstadt, Germany,e-mail: Harry.Weber@hella.com

C. Schuster are with the Institut für Theoretische Elektrotechnik, Hamburg University of Technology (TUHH), Hamburg, Germany

Weber, Baran, Utermöhlen and Schuster, "Macromodeling of Mutual Inductance for Displaced Coils Based on Laplace's Equation," in IEEE Transactions on Instrumentation and Measurement, vol. 70, pp. 1-11, 2021, Art no. 9506911, doi: 10.1109/TIM.2021.3063758

methods exist in order to obtain such macro models for different applications [10].
In [11], Polynomial Chaos Expansion is used for the efficient analysis of a multi-coil system deriving a series expansion in a desired parameter region. Furthermore, it is possible to derive a macro model by model order reduction or solving a fitting problem [10]. For example, a partial element equivalent circuit (PEEC) can be deduced by an electric field integral equation (EFIE) yielding a high dimensional problem which is reduced by model order reduction [12].
In [13], [14] a series expansion of the mutual inductance for arbitrary displacements of spiral coils is derived based on a given solution for a specific variation of position. The extension of a given solution to arbitrary displacements is obtained by treating the mutual inductance as a potential function in dependency of the relative position of the coils which obeys Laplace's equation. However, the presented method can only be applied for simple geometries for which an analytic solution can be derived in advance.
In this contribution, a more general method is presented to derive a macro model of the mutual inductance for filamentary coils in dependency of the relative position as shown in [15]. In contrast to the procedure described in [13], [14], it is possible to apply the presented method for complex coil geometry since no analytic solution of the mutual inductance is necessary.
Based on the idea to treat the mutual inductance as a potential function in the case of filamentary coils, a macro model approach is derived by solving Laplace's equation. Once suitable boundary conditions are used, the mutual inductance with respect to the relative position can be described by the macro model. An extension of the method for coils with cross section can be performed by discretization as presented in [16]. The advantage of the proposed method is the application independent of the specific coil geometry. Therefore, the proposed method can be applied in a variety of inductive applications in order to obtain a simple model of the mutual inductance in dependency of the relative positions of a pair of coils. Such macro model can be for example used in the design of position sensors, see for example [17], or for analysis of a complete system considering displacement of coils. In comparison to already existing methods, no analytic solution has to be known in advance and numerical or measurement results can be used in order to derive a macro model. The remainder of this contribution is structured as follows.
In Section II, the relation between mutual inductance and Laplace's equation is discussed and reviewed. The procedure to derive the macro model is presented and discussed in Section III. Possible adaption of the obtained general solution to given boundary conditions is discussed in Section IV. Finally, the complete procedure is demonstrated by means of examples from different areas of applications in Section VI in order to emphasize the broad applicability of the presented method.

II. Mutual Inductance as Potential Function

In Fig. 1, the considered arrangement of two filamentary coils with arbitrary geometry is presented. Each coil is described in correspondence to a separated axis with origins $\mathbf{O}_1$ and $\mathbf{O}_2$ by the parameterization $\mathbf{x}_1$ and $\mathbf{x}_2$. The distance between $\mathbf{O}_2$ and $\mathbf{O}_1$ is described by $\mathbf{R}$ with the direction from $\mathbf{O}_2$ to $\mathbf{O}_1$. In the following, the mutual inductance L_{12} shall be determined in a predefined region Ω with the boundary $\partial\Omega$. Therefore, it follows $\mathbf{R} \in \Omega$. The mutual inductance L_{12} between coil 1 and 2 can be calculated by the Neumann formula

$$L_{12} = \frac{\mu}{4\pi} \oint_{C_2} \oint_{C_1} \frac{\mathrm{d}\mathbf{x}_1 \cdot \mathrm{d}\mathbf{x}_2}{\|\mathbf{x}_1 - \mathbf{x}_2 + \mathbf{R}\|}, \tag{1}$$

whereby $\mathrm{d}\mathbf{x}_1$ and $\mathrm{d}\mathbf{x}_2$ are the differential flows of the currents in coil 1 and coil 2, respectively [18]. As can be seen in (1), a singularity can occur with respect to $\mathbf{R}$. The valid region of $\mathbf{R}$ depends on C_1, C_2, $\mathbf{x}_1$ and $\mathbf{x}_2$ or the origins $\mathbf{O}_1$ and $\mathbf{O}_2$, respectively. It has to be ensured that an intersection cannot occur by choosing appropriate parameters and origins.
An analytic solution of the integral (1) can only be derived in simple cases. Therefore, for each $\mathbf{R}$, (1) has to be solved numerically. However, the mutual inductance in (1) can be interpreted as potential function in dependency of $\mathbf{R}$ fulfilling Laplace's equation

$$\Delta L_{12}(\mathbf{R}) = 0 \tag{2}$$

with boundary conditions and the argument $\mathbf{R}$ [14], [18]. This can be shown by substitution of (1) in (2) with an arbitrary coordinate system for $\mathbf{R}$. Therefore, the mutual inductance of displaced coils can be determined by solving Laplace's equation in (2). In contrast to (1), the problem in (2) depends only on the displacement vector $\mathbf{R}$. This enables to determine the mutual inductance in dependency of $\mathbf{R}$ without solving the complete problem repeatedly for different $\mathbf{R}$ in Ω. However, a unique solution of Laplace's equation is only obtained in combination with boundary conditions. These can be derived in advance by (1), numerical simulations or measurements. Hence, the dependency on the explicit geometry of the coils is contained in the boundary conditions.

III. Macro Model Approach Solving Laplace's Equation

A solution of Laplace's equation in (2) can be derived by different methods [18]. One possibility is the application of numerical methods like Finite Differences [19]. Alternatively, an analytic solution can be derived with the method of separation of variables. Hereby, the solution of Laplace's equation is stated by basis functions $\hat{L}_{l_1,l_2}$ yielding a series expansion

$$L_{12} = \sum_{l_1,l_2=0}^{\infty} C_{l_1,l_2} \hat{L}_{l_1,l_2} \tag{3}$$

which is truncated after an order $N_{\max}$ yielding an approximate solution of Laplace's equation. With the boundary conditions on $\partial\Omega$, the coefficients C_{l_1,l_2} in (3) can be determined. The basis functions in (3) depend on the coordinate system in which $\mathbf{R}$ is described. In this contribution, $\mathbf{R}(r, \theta, \varphi)$ is described by a spherical coordinate system yielding the mutual inductance $L_{12}(r, \theta, \varphi)$.
For a Cartesian or cylindrical coordinate system, a general problem is composed of 6 and 3 solutions respectively. Only

for symmetrical problems, the number of superimposed solutions can be reduced [20]. Based on (2) a spherical boundary condition for Laplace's equation can be stated as

$$L_{12}(a,\theta,\varphi) = f(\theta,\varphi) \tag{4}$$

with the radius a, $\theta \in [0,\pi]$ and $\varphi \in [0,2\pi]$. The function $f(\theta,\varphi)$ depends on the specific geometry of the pair of coils and the relative position. If no additional constraints are given, a can be freely chosen as long as no intersection of the pair of coils occur. As will be discussed in Section IV, the accuracy of the procedure depends on a and has to be chosen in dependency of the considered problem.

A general solution of (2) in the case of a spherical coordinate system is derived by separation of variables. For this purpose, the product approach

$$L_{12}(r,\theta,\varphi) = R(r)\Theta(\theta)\phi(\varphi) \tag{5}$$

is applied. In (5) the mutual inductance $L_{12}(r,\theta,\varphi)$ is separated in three unknown functions $R(r)$, $\Theta(\theta)$ and $\phi(\varphi)$. With (5), Laplace's equation in (2) can be transformed into separated ordinary differential equations which are solved in order to determine the unknown functions $R(r)$, $\Theta(\theta)$ and $\phi(\varphi)$. The general solution obtained by (5) is

$$\begin{aligned} L_{12}(r,\theta,\varphi) = \sum_{l_1=0}^{\infty} \left(\frac{r}{a}\right)^{l_1} \Bigg[\frac{1}{2} a_{0l_1} P_{l_1}(\cos(\theta)) \\ + \sum_{l_2=1}^{l_1} \left(a_{l_2 l_1}\cos(l_2\varphi) + b_{l_2 l_1}\sin(l_2\varphi)\right) P_{l_1}^{l_2}(\cos(\theta)) \Bigg] \end{aligned} \tag{6}$$

inside the spherical boundary condition $r < a$ and

$$\begin{aligned} L_{12}(r,\theta,\varphi) = \sum_{l_1=0}^{\infty} \left(\frac{a}{r}\right)^{l_1+1} \Bigg[\frac{1}{2} a_{0l_1} P_{l_1}(\cos(\theta)) \\ + \sum_{l_2=1}^{l_1} \left(a_{l_2 l_1}\cos(l_2\varphi) + b_{l_2 l_1}\sin(l_2\varphi)\right) P_{l_1}^{l_2}(\cos(\theta)) \Bigg] \end{aligned} \tag{7}$$

outside the spherical boundary condition $r > a$, whereby $P_{l_1}(\cos(\theta))$ are Legendre polynomials, $P_{l_1}^{l_2}(\cos(\theta))$ are associated Legendre polynomials and $a_{l_2 l_1}, b_{l_2 l_1} \in \mathbb{R}$. A detailed derivation of the general solution and the convergence behavior of the series is described in [20].

For a pair of coils, (6) and (7) are applicable independent of the specific geometry. The missing coefficients $a_{l_2 l_1}$ and $b_{l_2 l_1}$ have to be adapted to the spherical boundary condition $f(\theta,\varphi)$ in (4). In comparison to the general solutions in (6) and (7), $f(\theta,\varphi)$ depends explicitly on the geometry of the coils. Hence, the complete problem has to be solved on the boundary condition.

Once the coefficients are adapted to the boundary condition, an appropriate macro model is given by (6) and (7) which describes the mutual inductance with respect to a position variation of the coils. In the next section, the calculation of the boundary conditions is discussed and possible methods for the adaption of the coefficients in (6) and (7) are described.

IV. Adaption of General Solution to Boundary Condition

An unique solution of (2) is only obtained in combination with boundary conditions. These have to be determined in advance for specific relative positions of the two coils. Hereby, boundary conditions correspond to values of L_{12} on a sphere with radius a from the origin $\mathbf{O}_2$ as shown in Fig. 1 for two given coils.

Different methods can be used to determine such boundary conditions. One possibility is to apply a field simulator or using measurement data. In order to reduce the effort further, Polynomial Chaos Expansion can be applied in these cases [11]. Additionally, (1) can be applied to derive boundary conditions numerically if a parameterization is possible.

In this contribution, two methods are discussed in order to adapt the macro model derived by separation of variables. One possibility is based on the fact that the basis functions $\hat{L}_{l_1,l_2}$ are orthogonal. Therefore, the coefficients C_{l_1,l_2} can be calculated directly using an appropriate scalar product. For the discussed spherical case in (6) and (7), the coefficients are calculated by

$$\begin{aligned} a_{l_2 l_1} = &\frac{(2l_2+1)(l_1-l_2)!}{2\pi(l_1+l_2)!} \int_0^{2\pi} \int_0^{\pi} f(\theta,\varphi) \cdot \\ &P_{l_1}^{l_2}(\cos(\theta)) \cos(l_2\varphi) \sin(\theta) \mathrm{d}\theta \mathrm{d}\varphi \end{aligned} \tag{8}$$

and

$$\begin{aligned} b_{l_2 l_1} = &\frac{(2l_2+1)(l_1-l_2)!}{2\pi(l_1+l_2)!} \int_0^{2\pi} \int_0^{\pi} f(\theta,\varphi) \cdot \\ &P_{l_1}^{l_2}(\cos(\theta)) \sin(l_2\varphi) \sin(\theta) \mathrm{d}\theta \mathrm{d}\varphi. \end{aligned} \tag{9}$$

If a parametrization of the coils can be given, $f(\theta,\varphi)$ can be represented by the Neumann formula in (8) and (9). This approach yields a multi dimensional integral which can be solved numerically. However, in general, rather complicated integral expressions are obtained yielding stability issues by applying standard numerical solvers. Additionally, for increasing l_1 and l_2 the evaluation time increases drastically.

Alternatively, boundary approximation methods can be utilized [21]. For this purpose, the series expansion in (6) and (7) is truncated after a certain order $N_{\max}$. The accuracy of the truncated series depends on the radius a of the spherical boundary condition and the geometry of a pair of coils. For values of a in the same size as the coil geometry, a larger variation of $f(\theta,\varphi)$ can be expected in comparison to smaller values of a. Hence, a larger maximal order $N_{\max}$ of the series expansion is necessary for the approximation of the mutual inductance. Further, it can be noticed from (6) that the contribution of higher order terms decreases with lower values of r. Therefore, better results in the vicinity of the origin ($r \ll a$) are expected if (6) is used as approach. In the case of (7), the contribution of the neglected higher order terms decreases for larger r yielding an opposite behavior as for (6). Therefore, (6) is suitable in the case of a description of the coils in the proximity of each other and (7) for a pair of coils at greater distance to each other. In all cases, it has to be ensured that no intersection occurs due to singularity in (1).

The main idea of the applied boundary approximation method is to represent the boundary condition by a series expansion [21]. The coefficients are calculated by solving a linear optimization problem. In this contribution, the truncated series in (3) obtained by the separation of variables is used as a physical based approach for the series expansion. The coefficients are calculated by minimizing the cost function

$$\min_{C_{l_1,l_2}} \sum_{i=1}^{N} \left(\sum_{l_1,l_2}^{N_{\max}} C_{l_1,l_2} \hat{L}_{l_1,l_2}(\mathbf{R}_i) - f(\theta_i,\varphi_i) \right)^2 \tag{10}$$

at discrete boundary points $\mathbf{R}_i \in \partial\Omega$ with a least square fit [22]. In the special case shown in (6) and (7) the following linear equation is solved

$$\mathbf{A}^\intercal \mathbf{A} \mathbf{C} = \mathbf{A}^\intercal \mathbf{y} \tag{11}$$

with

$$\mathbf{A} = \begin{pmatrix} \frac{1}{2} & \cdots & \sin(N_{\max}\varphi_1) P_{N_{\max}}^{N_{\max}}(\cos(\theta_1)) \\ \frac{1}{2} & \cdots & \sin(N_{\max}\varphi_2) P_{N_{\max}}^{N_{\max}}(\cos(\theta_2)) \\ \vdots & \ddots & \vdots \\ \frac{1}{2} & \cdots & \sin(N_{\max}\varphi_N) P_{N_{\max}}^{N_{\max}}(\cos(\theta_N)) \end{pmatrix}, \tag{12}$$

$$\mathbf{C} = (a_{00}, a_{0,1}, \cdots, b_{N_{\max}N_{\max}})^\intercal \tag{13}$$

and

$$\mathbf{y} = (f(\theta_1,\varphi_1), \cdots, f(\theta_N,\varphi_N))^\intercal . \tag{14}$$

In this contribution, the samples on the boundary condition are distributed equidistantly. In contrast to the scalar product in (8) and (9), sample points on the boundary obtained by measurement or simulation can be used. With (10), the missing coefficients in (6) and (7) are directly calculated so that a macro model of the mutual inductance with respect to the relative position is obtained. However, the possible maximal order depends on the number of points used. In [23], it is proposed to apply $N_1 > 2N_{\max}$ in the case of one independent variable in the least square fit, whereby N_1 describes the number of samples. Then, N_1 does not influence the accuracy of the least square fit anymore. Due to two independent variables in the presented method, the appropriate number of samples is $N = N_1 \cdot N_1 > (2N_{\max})^2$. Further, it shall be noticed that the coefficients obtained by the scalar product and the least square fit in (10) coincide only in special cases. In general, different coefficients are obtained by these two methods. A detailed convergence analysis of this method is discussed also in [23]. It is shown that with increasing $N_{\max}$ the approximation converges to the exact solution. By comparing the change of the coefficients with increasing $N_{\max}$, a sufficient maximal order can be estimated. Thereby, it has to be noticed that smaller order coefficients converges faster in comparison to higher order terms as shown in [23]. Therefore, a higher accuracy for small displacements $\|\mathbf{R}\| \approx 0$ are achieved in general.

V. Illustration of the Proposed Method by a Simple Example

In this section the complete procedure is described in the following by the simple example shown in Fig. 2. The example consists of two equal spiral coils with five windings and $r_{\text{in}} = 1\,\text{cm}$. In this example, the mutual inductance between two equal circular coils shall be calculated in dependency of the relative position. In order to provide an overview, each step of the procedure is summarized in Fig. 3. In the first step the origins $\mathbf{O}_1$ and $\mathbf{O}_2$ in relation to the two coils have to be defined which are used for the parametrization of each coil. The origins have to be placed so that for all possible $\mathbf{R}$ no intersection occurs between the pair of coils. In the special case shown in Fig. 2 both coils are assumed to be planar. In order to avoid intersection between both circular spiral coils an offset $\hat{z}$ is added. In the case of $\|\mathbf{R}\| = 0$, both origins are coincident and both circular spiral coils will not intersect with $\hat{z} \neq 0$. Therefore, an offset is added in order to avoid an intersection.

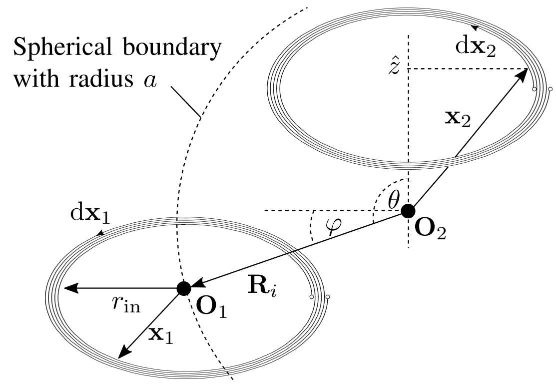

Fig. 2: Simple example consisting of two equal circular spiral coils with $r_{\text{in}} = 1\,\text{cm}$ and five windings.

In the next step, the spherical boundary condition $\partial\Omega$ with the radius a is defined. The radius a has to be chosen in such a way that in reference to the origins $\mathbf{O}_1$ and $\mathbf{O}_2$ no intersection between the pair of coils occur.In the case of the introductory example, the parameter a is restricted by $\hat{z}$. In the case of $a < \hat{z}$, an intersection is avoided for all parameters of φ and θ. In this example, the critical case occurs for $\theta = \pi\,\text{rad}$, that is coil 1 is moved in the direction of coil 2. If $a > \hat{z}$, then an intersection between both coils occur. Further, $f(\theta,\varphi)$ depends on a which is used for the least square fit. In dependency of the specific geometry of the pair of coils, the contributions of higher order depends on a. For smaller values of a, a lower maximal order is necessary. For example, in the case shown in Fig. 2 a suitable choice could be $a = r_{\text{in}}$ which corresponds to the radius of the structure.

Thirdly, an initial maximal order $N_{\max}$ is picked for the series expansion in (6). In the introductory example $N_{\max} = 1$ is chosen so that the mutual inductance is described by

$$\begin{aligned} L_{12} = \frac{1}{2}a_{00} + \left(\frac{r}{a}\right) \cdot \Big[&\frac{1}{2} a_{01} P_1(\cos(\theta)) \\ &+ (a_{11}\cos(\varphi) + b_{11}\sin(\varphi)) P_1^1(\cos(\theta)) \Big] . \end{aligned} \tag{15}$$

In the next step, $f(\theta_i,\varphi_i)$ is calculated at discrete positions $\mathbf{R}_i \in \partial\Omega$ on the spherical boundary with the radius a. Hereby, it has to be ensured that a sufficient number of samples is calculated for the given maximal order $N_{\max}$. In the case of $N > (2N_{\max})^2$, the accuracy of the applied least square fit

TABLE I: First largest coefficients of (6) for Fig. 2 obtained by (11).

$N_{\max}$	a_{00} [nH]	a_{01} [nH]	a_{02} [nH]	a_{03} [nH]
3	9.25	19.9428	56.0515	60.9788
5	6.66738	15.1316	27.658	32.6383
9	5.53311	12.9449	20.5171	25.7408
12	5.36795	12.7166	19.6271	25.1427
14	5.35047	12.6301	19.5362	24.9242

is independent of the number of samples. It is practically to pick at least enough samples so that the least square fit for $N_{\max}+2$ can be performed in order to evaluate the change of coefficients. For the considered case, this means that at least $N = 49$ is applied in order to evaluate the change of calculated coefficients with increasing order. Further, the mutual inductance on the boundary condition is calculated at equally distributed positions of φ_i and θ_i. With these values a least square fit as shown in (10) is performed in order to determine the missing coefficients in (6). A sufficient high $N_{\max}$ can be determined according to the change of the coefficients for increasing $N_{\max}$. If the change of coefficients is too large in comparison to the boundary values, the maximal order $N_{\max}$ has to be increased further. If necessary, the number of samples N on the boundary $\mathbf{R} \in \partial\Omega$ has to be increased as well in order to ensure $N > (2N_{\max})^2$. In the specific case of the pair of spiral coils, the least square fit is performed for the case of $N_{\max} = \{3, 5, 9, 12, 14\}$. Further, the coefficients for each maximal order are compared to each other and the difference between them are evaluated. In Table I, the first largest coefficients are presented for an exemplary set of parameters for the circular spiral coils. As can be seen, the difference between the coefficients for different maximal order reduces with increased $N_{\max}$. Further it can be seen that the lower order coefficients converge faster in comparison to the higher order terms. After determination of the coefficients, a macro model is obtained which describes the mutual inductance inside $r < a$ and outside $r > a$ of the spherical boundary condition. However, in this contribution only the mutual inductance inside $r < a$ of the spherical boundary condition is considered.

VI. Application to Different Coil Geometries

In this section, the described procedure is presented for different examples. For comparison of the obtained results the relative error

$$\text{rel. error} = \frac{|L_{12,\text{approx}} - L_{12,\text{num}}|}{|L_{12,\text{num}}|} \cdot 100\,\% \tag{16}$$

is considered whereby $L_{12,\text{approx}}$ are the results obtained by the derived macro model and $L_{12,\text{num}}$ are the numerical results obtained by repeatedly solving (1) using Gaussian quadrature. The presented procedure is applied to a coil system of a position sensor and a butterfly coil used in MRI.

A. Position Sensor

In this section, the described procedure is presented for a CIPOS® with the coil and rotor design shown in Fig. 4.

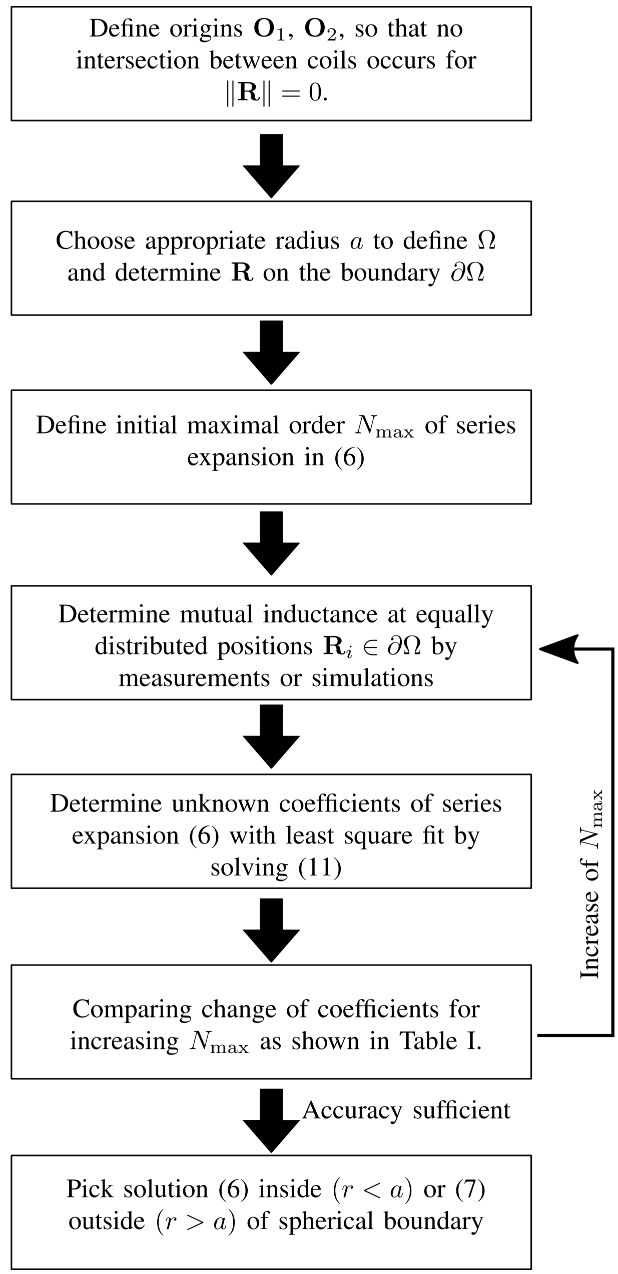

Fig. 3: Flowchart of the presented procedure applied in this contribution to derive a macro model of the mutual inductance for a pair of coils.

In particular, the mutual inductance between excitation coil and rotor is examined in detail which effects mainly the signal strength and therefore the signal-to-noise ratio. Additionally, the cross section of the conductors are reduced, since the procedure can only be applied for filamentary coils. An extension to coils with cross section can be performed by discretization for example.
In Fig. 5 the considered filamentary excitation and rotor coil are shown. In this specific case, the excitation coil is realized on a PCB on two layers. The macro model shall describe the behavior in the vicinity of the excitation coil. Therefore, (6) is used with a boundary condition of a radius a similar to the sizes of the excitation coil. Due to the possible singularity, as

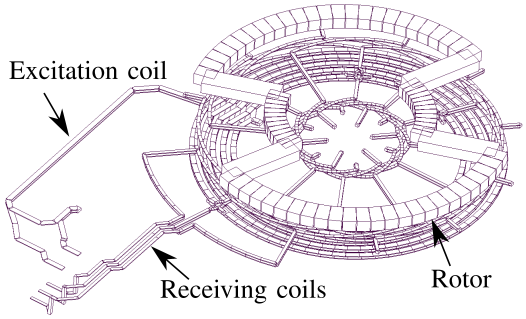

Fig. 4: Exemplary Contactless Inductive Position Sensor (CIPOS®) with excitation, receiving coil and rotor.

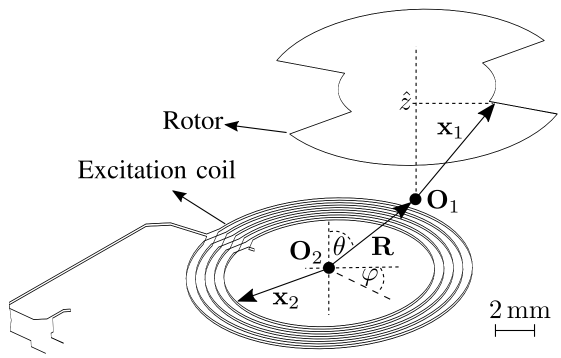

Fig. 5: Filamentary excitation coil and rotor of the CIPOS® in Fig. 4 with applied coordinate systems.

TABLE II: First largest coefficients of (6) for Fig. 5 in the case of $\hat{z} = 1\,\mathrm{cm}$ and $a = 0.9\,\mathrm{cm}$ obtained by (10).

$N_{\max}$	a_{00} [nH]	a_{01} [nH]	a_{02} [nH]	a_{03} [nH]
3	−25.88	40.146	−49.388	35.367
5	−24.884	39.034	−38.549	28.978
7	−24.774	38.912	−37.832	28.574
9	−24.761	38.899	−37.756	28.535

can be seen in (1), it has to be ensured that no intersection of the rotor and coil occur. For this reason, $a = 0.9\,\mathrm{cm}$ and an offset of $\hat{z} = 1\,\mathrm{cm}$ is used in order to ensure that the rotor is always above the excitation coil and no intersection is possible due to $r \leq a$. The equidistantly distributed data points on the boundary are obtained by an inhouse simulator based on a variation of PEEC [10]. In the next step, the least square fit in (10) is applied in order to obtain the missing coefficients in (6). In Table II, the first four largest coefficients are presented in dependency of the maximal order $N_{\max}$. As shown, the coefficients converging with increasing $N_{\max}$. This analysis can be used to determine a sufficient high maximal order $N_{\max}$. If the change of coefficients is low, a higher accuracy is obtained by the macro model. Additionally, the smaller the order of the coefficient the faster it converges.

In Fig. 6, the results obtained by the macro model for $r = 0.7\,\mathrm{cm}$ with $N_{\max} = 7$ (plane) in dependency of θ and φ are compared to numerical results (dots). The maximal relative error in the presented range is $0.99\,\%$. For a more specific evaluation, the results of the macro model are compared at specific positions in the following.

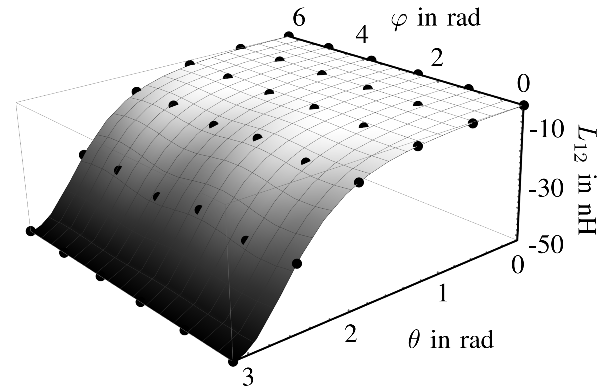

Fig. 6: Macro model results with $N_{\max} = 7$ (plane) for different positions at $r = 0.7\,\mathrm{cm}$ in comparison to numerical results (dots) for the coil system in Fig. 5.

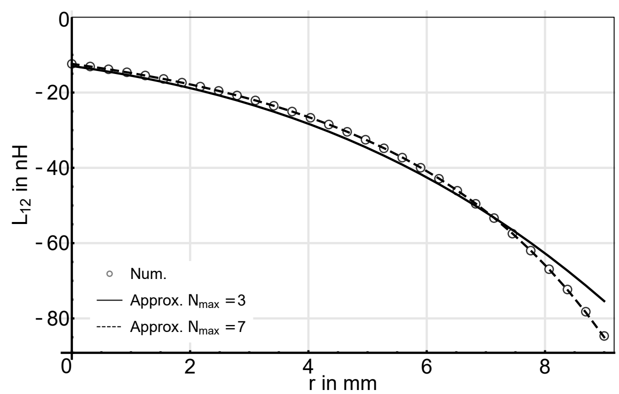

Fig. 7: Mutual inductance of rotor and excitation coil in Fig. 5 approximated by the macro model with $N_{\max} = 3$ (straight line) and $N_{\max} = 7$ (dashed line) in comparison to numerical results by inhouse simulator (dots) with $\theta = \pi\,\mathrm{rad}$, $\varphi = 0\,\mathrm{rad}$ and varied distance r.

TABLE III: Maximal relative error in Fig. 7 for different $N_{\max}$ in the case of $\hat{z} = 1\,\mathrm{cm}$ and $a = 0.9\,\mathrm{cm}$.

$N_{\max}$	Max. relative error in the range $r < 1.2\,\mathrm{mm}$	Max. relative error in the complete range
3	4.9 %	12.7 %
4	1.01 %	5.55 %
5	0.47 %	2.39 %
7	0.007 %	0.37 %

TABLE IV: Maximal relative error in the case of $\hat{z} = 2\,\mathrm{cm}$ and $a = 1.9\,\mathrm{cm}$ for a variation of r in the range from $1\,\mathrm{cm}$ to $1.9\,\mathrm{cm}$ at $\theta = \pi\,\mathrm{rad}$ and $\varphi = 0\,\mathrm{rad}$.

$N_{\max}$	Max. relative error in the range $1\,\mathrm{cm} < r < 1.9\,\mathrm{cm}$
3	52.29 %
4	30.71 %
5	18.49 %
7	13.97 %

In Fig. 7, the solution obtained by the macro model with $N_{\max} = 7$ is compared with numerical results obtained by

TABLE V: First largest coefficients of (6) for Fig. 5 in the case of $\hat{z} = 2\,\mathrm{cm}$ and $a = 1.9\,\mathrm{cm}$ obtained by (10).

$N_{\max}$	a_{00} [nH]	a_{01} [nH]	a_{02} [nH]	a_{03} [nH]
3	-8.2672	17.336	-42.797	43.2
5	-6.4587	14.317	-23.299	25.971
7	-6.0022	13.557	-20.361	23.5008

the inhouse simulator for a variation of r with $\theta = \pi\,\mathrm{rad}$ and $\varphi = 0\,\mathrm{rad}$. The maximal relative error is $0.37\,\%$ in the complete range for $N_{\max} = 7$. The influence of the maximal order $N_{\max}$ is shown in Table III. It can be noticed that with increasing $N_{\max}$ the maximal relative error decreases. Additionally, the relative error in the range of $0 < r < 1.2\,\mathrm{mm}$ is presented in comparison. The accuracy of the model is higher in the vicinity of the origin $r \approx 0$. For larger values of r, the error increases since the contribution of higher order terms increases as well which converge slower than the lower order terms. Therefore, a higher relative error is obtained in the larger range.

In Table IV, the same study is performed for a larger value of a. The variation of r is adapted to the range from $1\,\mathrm{cm}$ to $1.9\,\mathrm{cm}$ in order to remain the comparability to the results in Table III. A comparison of Table III and Table IV shows that for equal maximal order $N_{\max}$ the maximal relative error is higher in the case of a larger value of a.

In Table V, the first four largest coefficients are presented in dependency of the maximal order $N_{\max}$ for $\hat{z} = 2\,\mathrm{cm}$. In comparison to Table II, a larger change of coefficients can be noticed with increased $N_{\max}$. This indicates that $N_{\max} = 7$ is not sufficient enough and a larger $N_{\max}$ has to be used for the case $\hat{z} = 2\,\mathrm{cm}$. Therefore, the relative error is much higher in Table V in comparison to Table II. Due the power series characteristics, the relative error is higher for $a = 2\,\mathrm{cm}$ since a larger value of r is used in comparison to the results with $a = 0.9\,\mathrm{cm}$. Therefore, the contribution of the slower converging coefficients is increased, too.

The results obtained by the macro model with $N_{\max} = 7$ (straight line) and $N_{\max} = 4$ (dashed line) are compared to numerical results (dots) for $r = 0.7\,\mathrm{cm}$ and $\varphi = 0\,\mathrm{rad}$ in Fig. 8. In this case, a maximal relative error of about $1.25\,\%$ is reached. The behavior for a variation of φ at $r = 0.8\,\mathrm{cm}$ and $\theta = \frac{\pi}{2}$ is shown in Fig. 9. Hereby, the macro model with $N_{\max} = 7$ (straight line) is compared to numerical results (dots). In this case, the maximal relative error is about $2.93\,\%$. In [17] a fit is used to approximate the magnetic field for two perfectly axial aligned solenoid coils. In this case, an error lower than $0.1\,\mathrm{cm}$ for a distance from $4\,\mathrm{cm}$ up to $0.8\,\mathrm{m}$ is achieved with the fit. In contrast to the results in [17], the presented method can be also applied for more complex coil geometries as shown in Fig. 5. Further, the not axial case can be modeled which enables the detection in all three directions. However, a much higher order is necessary in order to achieve higher accuracy. In the following subsection, the procedure is demonstrated for a different coil geometry from a different area of application in order to demonstrate the broad applicability.

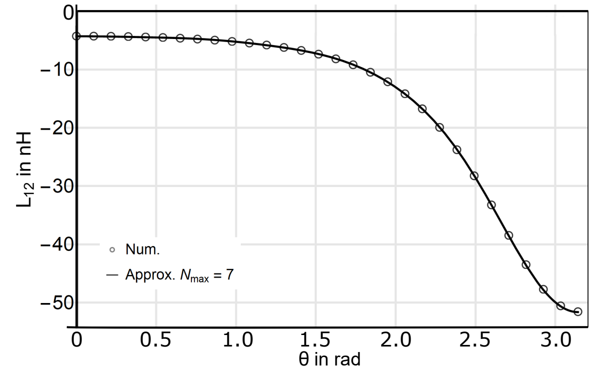

Fig. 8: Mutual inductance of rotor and excitation coil in Fig. 5 approximated by the macro model (straight line) in comparison to numerical results by inhouse simulator (dots) with $r = 0.7\,\mathrm{cm}$, $\varphi = 0\,\mathrm{rad}$ and varied distance r.

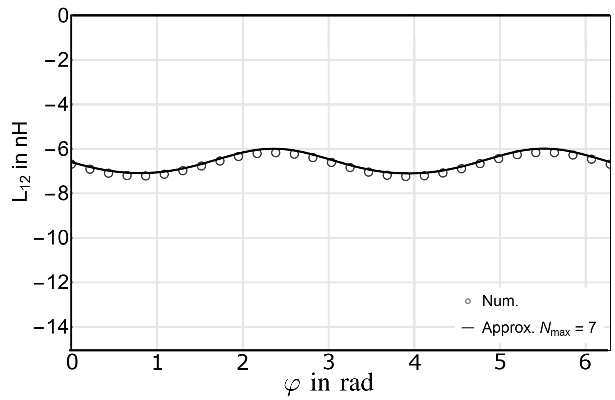

Fig. 9: Mutual inductance of rotor and excitation coil in Fig. 5 approximated by the macro model (straight line) in comparison to numerical results by inhouse simulator (dots) with $r = 0.8\,\mathrm{cm}$, $\theta = \pi/2\,\mathrm{rad}$ and varied distance r.

B. Example: Rogowski Coil

In this section the described method is applied for a Rogowski coil in Fig. 10 which can be used for the measurement of alternating current [24]. The origins $\mathbf{O}_1$ for a Rogowski coil and $\mathbf{O}_2$ for a wire, which passes through the axes of the Rogowski coil, are in the center of each coil as shown in Fig. 10a. In the case of $\|\mathbf{R}\| = 0$ both origins are equal. The geometric parameters of the Rogowski coil are $R_{\mathrm{in}} = 2\,\mathrm{mm}$, $d = 2.5\,\mathrm{mm}$ and $h = 1.2\,\mathrm{mm}$ with $N = 20$ windings. The length of the wire is $l = 5\,\mathrm{mm}$ so that a movement in z-direction has no significant impact on the mutual inductance. For the presented procedure a radius of $a = 1.4\,\mathrm{mm}$ is used for the boundary condition. Due to $r \leq a < R$, no intersection between wire and Rogowski coil can occur. The mutual inductance between wire and Rogowski coil are calculated by using an inhouse simulator based on a variation of PEEC. In Table VI, the first largest coefficients are shown in dependency of $N_{\max}$, which are obtained by the least square fit. At $N_{\max} = 7$, a small change in comparison to the boundary values of the coefficients with increasing $N_{\max}$ can be noticed. For this reason, $N_{\max} = 7$ is used in the following.

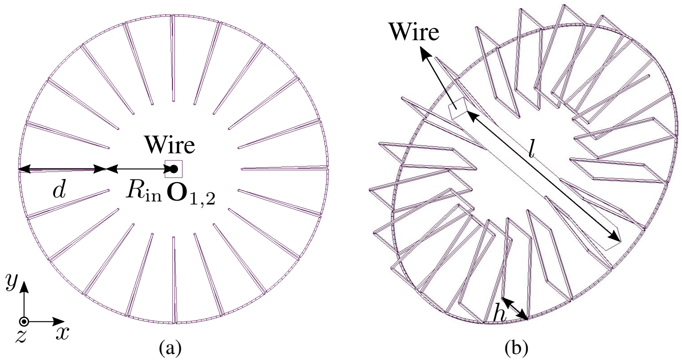

Fig. 10: Rogowski coil realized on a PCB with a current wire inside of the coil in the top (a) and side view (b) [24].

TABLE VI: First largest coefficients of (6) $a = 1.9\,\mathrm{cm}$ for Fig. 10 obtained by (10).

$N_{\max}$	a_{00} [nH]	a_{01} [nH]	a_{02} [nH]
1	4.9303	0.47163	-
3	5.0909	0.47520	-0.54948
5	5.0903	0.47633	-0.55576
7	5.0902	0.47631	-0.55626

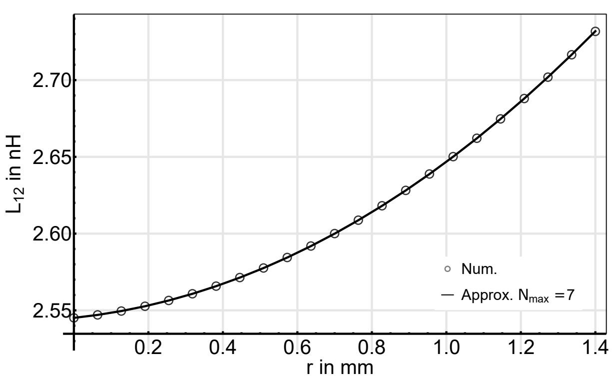

Fig. 11: Mutual inductance between Rogowski coil and wire calculated by the macro model (line) and numerical simulations (points) for $\varphi = 0\,\mathrm{rad}$ and $\theta = \pi/2\,\mathrm{rad}$.

In Fig. 11, the results in dependency of $r \leq a$ obtained by the macro model for $\theta = \pi/2\,\mathrm{rad}$ and $\varphi = 0\,\mathrm{rad}$ are shown1. The maximal error in the complete range is about $0.004\,\%$. In the next step, a variation of θ is considered for $r = 1\,\mathrm{mm}$ and $\varphi = 0\,\mathrm{rad}$. In Fig. 12, the results obtained by the macro model (line) are compared to numerical results (points). The maximal relative error is about $0.0025\,\%$. As presented, the macro model yields high accuracy with a relative error lower than $0.01\,\%$. Due to the symmetry of the coil system, a much higher accuracy in comparison to the example discussed in Section VI-A are obtained with the same maximal order.

C. Example: Butterfly Coils

In this section, the procedure is demonstrated for two identical coils with the shape shown in Fig. 13 and the arrangement demonstrated in Fig. 14. In the literature this coil design is known as butterfly coils, due to the structure similar to a

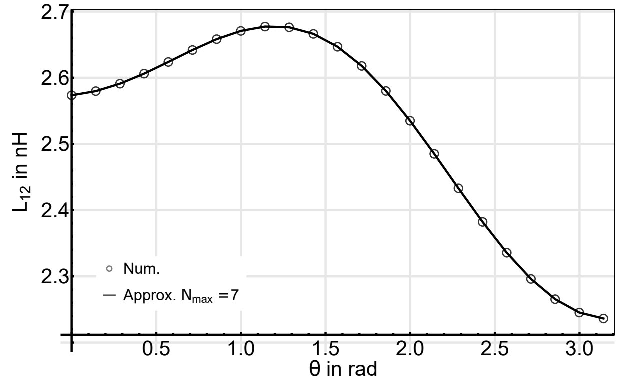

Fig. 12: Mutual inductance between Rogowski coil and wire calculated by the macro model (line) and numerical simulations (points) for $\varphi = 0\,\mathrm{rad}$ and $r = 1\,\mathrm{mm}$.

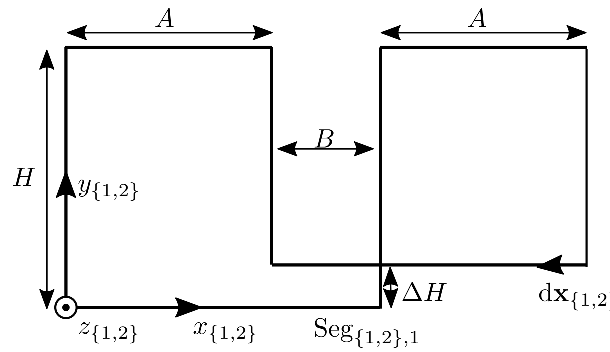

Fig. 13: Description of a butterfly coil in a Cartesian coordinate system applied in an array with identical coils for MRI with $A = 11\,\mathrm{cm}$, $B = 4\,\mathrm{cm}$, $H = 1\,\mathrm{cm}$ and $\Delta H = 1\,\mathrm{cm}$ [25].

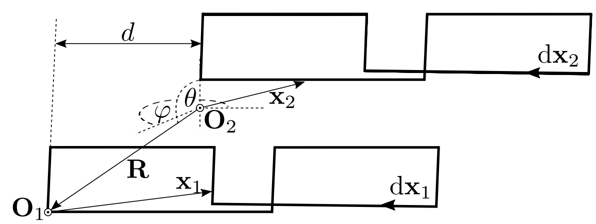

Fig. 14: Array of two equal butterfly coils applied in MRI with variable relative positions to each other described in a spherical coordinate system [25].

butterfly [25]. $\mathbf{O}_1$ and $\mathbf{O}_2$ are the corresponding origins of coil 1 and 2, respectively. The dimensions of the coils are $A = 11\,\mathrm{cm}$, $B = 4\,\mathrm{cm}$, $H = 14\,\mathrm{cm}$ and $\Delta H = 1\,\mathrm{cm}$ [25]. In this example, the second coil is considered always above the first coil. Therefore, the procedure is performed with (6) and for the parameterization of the coils, a Cartesian coordinate system is used. For example, the denoted segments in Fig. 13 are described by

$$\mathbf{r}_{\mathrm{Seg}_{1,1}} = [\tilde{x}_1 \; 0 \; 0]^{\mathsf{T}} \quad \tilde{x}_1 \in [0, A+B] \tag{17}$$

and

$$\mathbf{r}_{\mathrm{Seg}_{2,1}} = [\tilde{x}_2 \; 0 \; \hat{z}]^{\mathsf{T}} \quad \tilde{x}_2 \in [0, A+B] \tag{18}$$

in reference to the corresponding origins $\mathbf{O}_1$ and $\mathbf{O}_2$, respectively. In (18), an additional offset $\hat{z}$ is added in order to ensure that the second coil is always placed above the

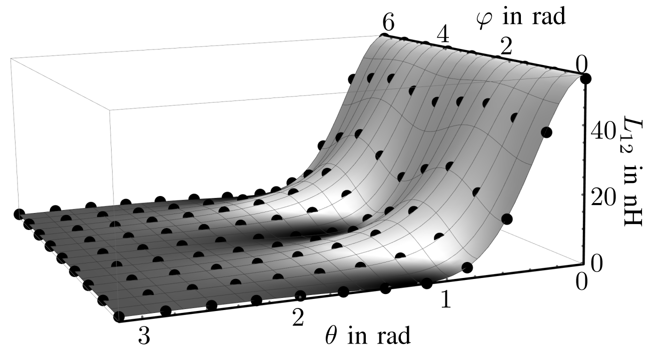

Fig. 15: Macro model results with $N_{\max} = 14$ (plane) for different positions at $r = 12\,\text{cm}$ in comparison to numerical results (dots) for the coil system in Fig. 14.

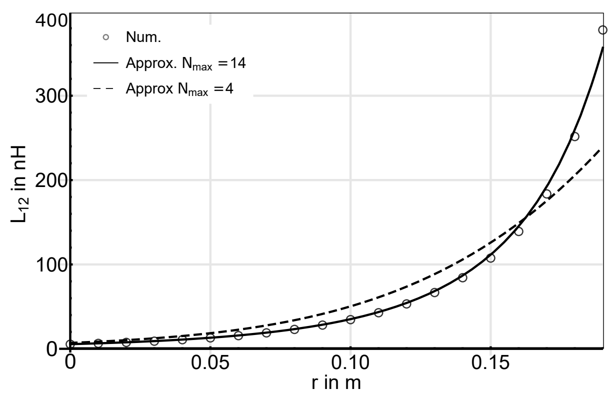

Fig. 16: Macro model results with $N_{\max} = 4$ (dashed line) and $N_{\max} = 14$ (straight line) for a variation of r at $\theta = 0\,\text{rad}$ and $\varphi = 0\,\text{rad}$ in comparison to numerical results (dots) for the coil system in Fig. 14.

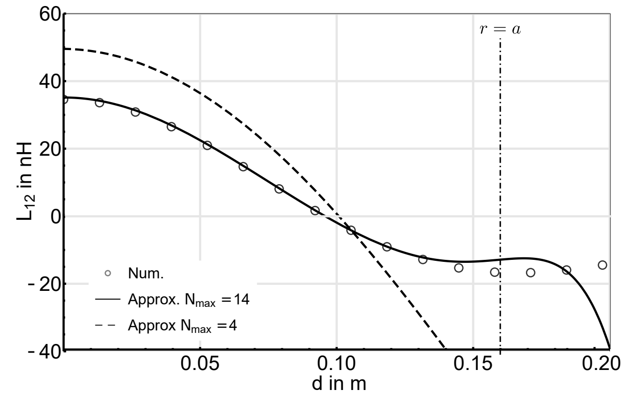

Fig. 17: Macro model results with $N_{\max} = 4$ (dashed line) and $N_{\max} = 14$ (straight line) for a variation of d with a height distance between the coils of $10\,\text{cm}$ at $\varphi = 0\,\text{rad}$ in comparison to numerical results (dots) for the coil system in Fig. 14.

TABLE VII: Maximal relative error in Fig. 16 for different $N_{\max}$ in the case of $\hat{z} = 20\,\text{cm}$ and $a = 19\,\text{cm}$.

$N_{\max}$	Max. relative error
4	47.4 %
6	22.1 %
8	14.4 %
10	10.2 %
12	7.56 %
14	5.6 %

TABLE VIII: Maximal relative error in the case of $\hat{z} = 11\,\text{cm}$ and $a = 10\,\text{cm}$ for a variation of r in the range from $0\,\text{cm}$ to $10\,\text{cm}$ at $\theta = 0\,\text{rad}$ and $\varphi = 0\,\text{rad}$.

$N_{\max}$	Max. relative error
4	18.79 %
6	10.72 %
8	6.88 %
10	4.58 %
12	3.08 %
14	2.07 %

first one. With the restriction $\hat{z} > a$, it is also assured that no intersection between both coils is possible during the calculation of the boundary samples. In this example, the offset is set to $\hat{z} = 20\,\text{cm}$ and the radius is chosen as $a = 19\,\text{cm}$. All results are compared to solutions obtained by a repetitive evaluation of (1) for the corresponding $\mathbf{R} \in \partial\Omega$. For this, an equidistant grid on the boundary is used.

In Fig. 15, the results obtained by the macro model for $r = 12\,\text{cm}$ with $N_{\max} = 14$ (plane) in dependency of θ and φ are compared to numerical results (dots). The maximal relative error in the presented range is $17.85\,\%$ with $N_{\max} = 14$. For a better comparison, different position variations of the coils are examined in the following.

In Fig. 16, the mutual inductance calculated by the macro model with $N_{\max} = 14$ (straight line) and $N_{\max} = 4$ (dashed line) in comparison to numerical results (dots) is shown for $\theta = 0\,\text{rad}$ and $\varphi = 0\,\text{rad}$. This position variation reduces the distance between the coils. The deviation of the results obtained by the macro model increases with r as expected. Further, it can be noticed that the increase of the maximal order $N_{\max}$ yields a better approximation for larger r. The maximal relative error is $47.4\,\%$ for $N_{\max} = 4$ and $5.6\,\%$ for $N_{\max} = 14$. An overview of the maximal relative error in dependency of $N_{\max}$ is shown in Table VII. With increasing order, the maximal relative error decreases. However, the change of relative error decreases with larger $N_{\max}$. In Table VIII, the same investigation is performed for $a = 10\,\text{cm}$. In order to ensure the same distance between the coils, the parameterization in (18) is adapted to $\hat{z} = 11\,\text{cm}$. A comparison between Table VII and VIII shows that the maximal relative error decreases in the case of $a = 10\,\text{cm}$ at the same maximal order $N_{\max}$. However, the possible range of r is more restricted in the case of $a = 10\,\text{cm}$. Therefore, the original parameters $\hat{z} = 20\,\text{cm}$ and $a = 19\,\text{cm}$ are used in the following. In Fig. 17, the behavior for a variation of d with $\varphi = 0\,\text{rad}$ is presented for $N_{\max} = 4$ (dashed line) and $N_{\max} = 14$ (straight line) in comparison to numerical results (dots). For an increasing maximal order $N_{\max}$, the accuracy of the macro model increases. At $d = 16.16\,\text{cm}$, it follows $r = a$, so that the macro model cannot be applied for larger values anymore. Nevertheless, the optimal distance d at which the magnetic coupling between the two coils is minimized can be directly obtained by the macro model inside the boundary condition with $r < a$ [26]. The maximal relative error is $360.13\,\%$ for $N_{\max} = 4$ and $12\,\%$ for $N_{\max} = 14$ in the region $r < a$.

In summary, it can be noticed that the macro model provides better approximation for smaller r as expected. The accuracy can be increased by the maximal order $N_{\max}$.

VII. Conclusion

In this contribution, a new method is presented for the macro modeling of the mutual inductance of two filamentary coils in dependency of the relative position. Instead of repeatedly solving the complete problem for different positions, the mutual inductance is treated as a potential function which obeys Laplace's equation. An approximate solution is obtained by a series expansion in spherical coordinates based on the separation of variables approach for Laplace's equation. The unknown coefficients of the approach are adapted by a least square fit. Thereby, the mutual inductance has only to be calculated at specific positions of the two filamentary coils. The complete procedure is presented by means of different examples which are applied in biomedical and industrial applications. Depending on the pair of coils and the considered region Ω, a sufficient maximal order of the series expansion has to be used for a given accuracy. It was shown, that the accuracy of the presented method depends on the specific coil geometry. A possibility to determine a suitable maximal order was also presented by comparing the calculated coefficients with increasing maximal order. Due to the linearity of the considered problem, the method can also be applied for systems containing more than two coils. For this purpose, the method is applied to every possible pair of coils separately. After that, the mutual inductance between every pair of coils in the system can be described. In following contributions, the benefits of the application of numerical methods to solve the Laplace's equation can be examined. Additionally, the possibility to reduce the effort for the calculation of the boundary condition with known order reduction techniques like PCE can be researched.

References

[1] B. Aschenbrenner and B. G. Zagar, "Analysis and validation of a planar high-frequency contactless absolute inductive position sensor," *IEEE Transactions on Instrumentation and Measurement*, vol. 64, 2014.

[2] A. Grima, M. D. Castro, A. Masi, and N. Sammut, "Design enhancements of an ironless inductive position sensor," *IEEE Transactions on Instrumentation and Measurement*, vol. 69, 2020.

[3] V. Pasku, A. D. Angelis, M. Dionigi, A. Moschitta, G. D. Angelis, and P. Carbone, "Analysis of nonideal effects and performance in magnetic positioning systems," *IEEE Transactions on Instrumentation and Measurement*, vol. 65, 2016.

[4] N. Anandan and B. George, "Design and development of a planar linear variable differential transformer for displacement sensing," *IEEE Sensors Journal*, vol. 17, no. 16, pp. 5298–5305, aug 2017.

[5] N. Labahn, F. Utermöhlen, and H. Weber, *Hochintegrierte Motorpositionssensoren für Bremssysteme und elektrische Antriebe*. Berlin, Heidelberg: Springer Berlin Heidelberg, 2020, pp. 325–344.

[6] J. Anders and K. Lips, "Mr to go," *Journal of Magnetic Resonance*, vol. 306, pp. 118 – 123, 2019. [Online]. Available: http://www.sciencedirect.com/science/article/pii/S1090780719301314

[7] F. C. Flack, E. D. James, and D. M. Schlapp, "Mutual inductance of air-cored coils: Effect on design of radio-frequency coupled implants," *Medical & Biological Engineering*, vol. 9, no. 2, pp. 79–85, mar 1971.

[8] S. Babic, J. Martinez, C. Akyel, and B. Babic, "Mutual inductance calculation between misalignment coils for wireless power transfer of energy," *Progress In Electromagnetics Research M*, vol. 38, 2014.

[9] M. Soma, D. C. Galbraith, and R. L. White, "Radio-frequency coils in implantable devices: Misalignment analysis and design procedure," *IEEE Transactions on Biomedical Engineering*, vol. BME-34, no. 4, pp. 276–282, apr 1987.

[10] Grivet-Talocia and Gustavsen, "Black-box macromodeling and its EMC applications," *IEEE Electromagnetic Compatibility Magazine*, vol. 5, no. 3, pp. 71–78, 2016.

[11] Z. Wen, Q. Wu, O. F. Yildiz, and C. Schuster, "Design of experiments for analyzing the efficiency of a multi-coil wireless power transfer system using polynomial chaos expansion," in *2019 Joint International Symposium on Electromagnetic Compatibility*, 2019.

[12] T.-S. Nguyen, T. L. Duc, T.-S. Tran, J.-M. Guichon, O. Chadebec, and G. Meunier, "Adaptive multipoint model order reduction scheme for large-scale inductive PEEC circuits," *IEEE Transactions on Electromagnetic Compatibility*, vol. 59, no. 4, pp. 1143–1151, aug 2017.

[13] S. Butterworth, "On the coefficients of mutual induction of eccentric coils," *Philosophical Magazine*, vol. 6, 1916.

[14] C. Snow, "The mutual inductance of two parallel circles," *Bureau of Standards Journal of Research*, vol. 3, 1929.

[15] H. Baran, "Modellreduktion der elektromagnetischen Charakterisierung eines induktiven Positionssensors für die Automobilindustrie," Master's thesis, TUHH Technische Universität Hamburg, 2020.

[16] S. Babic, C. Akyel, and J. Martinez, "A new formula for calculating the magnetic force between two caoxial thick circular coils with rectangular cross-section," *Journal of Electromagnetic Waves and Applications*, 2015.

[17] P. Ripka and A. Zikmund, "Magnetic tracker with high precision," *Proc. Eurosensors XXV*, 2011.

[18] J. D. Jackson, *Classical Electrodynamics*, 3rd ed. John Wiley & Sons, Inc., 1999.

[19] J. S. Hornsby, "A computer programme for the solution of elliptic partial differential equations:potential problems," *Geneva:CERN*, 1963.

[20] R. P. Agarwal and D. O. Regan, *Ordinary and Partial Differential Equations With Special Functions, Fourier Series, and Boundary Value Problems*. Springer Science+Business Media, LLC, 2009.

[21] F. Read, "A collocation method for solving laplace's equation," *Journal of Computational Physics*, vol. 6, no. 3, pp. 527 – 532, 1970. [Online]. Available: http://www.sciencedirect.com/science/article/pii/002199917090046X

[22] I. Griva, S. G. Nash, and A. Sofer, *Linear and nonlinear optimization*. Siam, 2009, vol. 108.

[23] A. Arad, Z. Yosibash, G. Ben-Dor, and A. Yakhot, "Computing flux intensity factors by a boundary method for elliptic equations with singularities," *Communications in Numerical Methods in Engineering*, vol. 14, no. 17, 1998.

[24] J. N. Fritz, C. Neeb, and R. W. D. Doncker, "A pcb integrated differential rogowski coil for non-intrusive current measurements featuring high bandwidth and dv/dt immunity," *Power and Energy Student Summit (PESS)*, 2015.

[25] G. Giovannetti, V. Viti, V. Positano, M. F. Santarelle, L. Landini, and A. Benassi, "Magnetostatic simulation for accurate design of low field mri phased-array coils," *Concepts in Magnetic Resonance Part B: Magnetic Resonance Engineering: An Educational Journal*, vol. 31, no. 3, 2007.

[26] B. Gruber, M. Froeling, T. Leiner, and D. W. Klomp, "Rf coils: A practical guide for nonphysicists," *Journal of Magnetic Resonance Imaging*, vol. 48, no. 3, 2018.